Design and mechanical evaluation of a novel dynamic growing rod to improve the surgical treatment of Early Onset Scoliosis

Alvarez, Alba Gonzalez; Dearn, Karl D.; Lawless, Bernard M.; Lavecchia, Carolina E.; Vommaro, Francesco; Martikos, Konstantinos; Greggi, Tiziana; Shepherd, Duncan E.t.

DOI:
10.1016/j.matdes.2018.06.008

Document Version
Peer reviewed version

Citation for published version (Harvard):
Alvarez, AG, Dearn, KD, Lawless, BM, Lavecchia, CE, Vommaro, F, Martikos, K, Greggi, T & Shepherd, DET 2018, 'Design and mechanical evaluation of a novel dynamic growing rod to improve the surgical treatment of Early Onset Scoliosis', *Materials and Design*, vol. 155, pp. 334-345.
https://doi.org/10.1016/j.matdes.2018.06.008

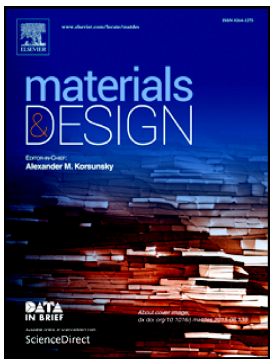

Design and mechanical evaluation of a novel dynamic growing rod to improve the surgical treatment of Early Onset Scoliosis

Alba Gonzalez Alvarez, Karl D. Dearn, Bernard M. Lawless, Carolina E. Lavecchia, Francesco Vommaro, Konstantinos Martikos, Tiziana Greggi, Duncan E.T. Shepherd

PII: S0264-1275(18)30477-5
DOI: doi:10.1016/j.matdes.2018.06.008
Reference: JMADE 3978

To appear in: *Materials & Design*

Received date: 3 April 2018
Revised date: 23 May 2018
Accepted date: 5 June 2018

Please cite this article as: Alba Gonzalez Alvarez, Karl D. Dearn, Bernard M. Lawless, Carolina E. Lavecchia, Francesco Vommaro, Konstantinos Martikos, Tiziana Greggi, Duncan E.T. Shepherd , Design and mechanical evaluation of a novel dynamic growing rod to improve the surgical treatment of Early Onset Scoliosis. Jmade (2017), doi:10.1016/j.matdes.2018.06.008

Title:

DESIGN AND MECHANICAL EVALUATION OF A NOVEL DYNAMIC GROWING ROD TO IMPROVE THE SURGICAL TREATMENT OF EARLY ONSET SCOLIOSIS

Authors:

Alba Gonzalez Alvarez[1], Karl D. Dearn[1], Bernard M. Lawless[1], Carolina E. Lavecchia[1], Francesco Vommaro[2], Konstantinos Martikos[2], Tiziana Greggi[2], Duncan E.T. Shepherd[1]

[1:] Department of Mechanical Engineering, School of Engineering, University of Birmingham, United Kingdom

[2:] Department of Spinal Deformity Surgery, Rizzoli Orthopaedic Institute, Bologna, Italy

Reference for the article: **JMADE 3978**

DESIGN AND MECHANICAL EVALUATION OF A NOVEL DYNAMIC GROWING ROD TO IMPROVE THE SURGICAL TREATMENT OF EARLY ONSET SCOLIOSIS

1. INTRODUCTION

Early Onset Scoliosis (EOS) is a severe abnormal curvature of the spine diagnosed at the age of ten years or less (Choudhury et al., 2017). Growing rods are the gold standard surgical treatment of EOS (Cunin, 2014). These implants have been developed to correct spinal deformity while guiding spinal growth (Greggi et al., 2012; Cunin, 2014) so that the growth potential of the spine and lungs is preserved in paediatric patients. Growing rods are expandable devices that are inserted through the back of the child (subcutaneously or intramuscularly (Oetgen et al, 2012)) and placed within the concavity of the curved spine (when a single rod is used) or on both sides (double construction). They can be anchored to the ribs and/or vertebrae by way of hooks and/or screws. Different constructions are possible depending on the curvature of the patient. After implantation, a periodical lengthening procedure is required in order to elongate the device and gradually correct the curvature of the spine (Odent et al., 2015) (figure 1).

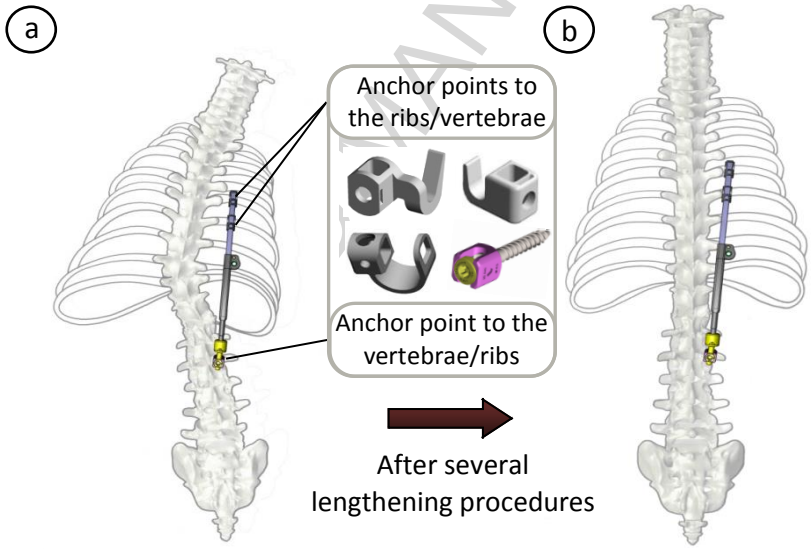

***Figure 1**- An example of the surgical treatment of Early Onset Scoliosis (EOS) with a growing rod. a) Scoliotic spine with growing rod implanted. b) Straight spine after several implant elongations. Different anchor systems including hooks or screws are also shown.*

Growing rods are associated with a highly variable range of complications (Greggi et al., 2012) which rate differs from 29% (Thompson et al., 2005) to 72% (Teoh et al., 2016; Sankar et al., 2010). The most common complications occurring are implant-related problems (such as rod fractures) and skin infections due to several surgeries being performed over the course of the treatment (Sankar et al., 2010; Akbarnia et al., 2016). This paper describes the development of a novel growing rod device that aims to improve the surgical treatment of EOS.

2. DESIGN SPECIFICATION

The main design consideration was that the implant should be able to mechanically correct three-dimensional spinal deformities (both in the frontal and sagittal anatomical planes) in skeletally immature patients while keeping the lowest dimensional profile. The device should:

- Allow 60 mm of elongation, considering that the maximum mean growth of spinal instrumented area during treatment has been reported to vary from 46.7 mm (Akbarnia et al., 2005) to 57 mm (Akbarnia et al., 2008).
- Include a rod with the lowest possible dimensional profile and a maximum diameter of 5 mm to prevent implant prominence over the skin of patients.
- Provide manual distraction so that surgeons can feel the stiffness of the patient's spine and elongate the device accordingly, achieving a controlled length of expansion.
- Provide minimally invasive surgery for distraction procedures to reduce skin and wound infections. The smaller the surgical incision the better.
- Be elongated from the same point so that the skin opening position for surgery is known and the exposure of the patient to repetitive X-Rays is avoided.
- Reduce the recurrent implant complication of rod breakage that occurs with current devices. Rod breakage is caused by fatigue bending compressive loads occurring during flexion motion of the patient (Hill et al., 2017). The VEPTR I device (Depuy Synthes Spine, Raynham, MA, USA) is one of the most used implants in the surgery of EOS (Odent et al., 2015). For further information relating to the VEPTR I see: DePuy Synthes Spine, (2016) and Akbarnia et al., (2016). This implant has been reported to provide fatigue strength of 100 N with the test running-out at 5 million cycles at 5 Hz (Food and Drug Administration, 2004). Therefore, the novel device should improve this value.
- Provide a maximum length of 180-220 mm which is the thoracic spinal height that should be reached at skeletal maturity in order to avoid respiratory insufficiency (Akbarnia et al., 2016; Karol et al., 2008). The maximum length provided by the VEPTR I device is 220 mm corresponding to a rib-sacrum construction (Food and Drug Administration, 2004). The novel device should provide a length of 190 mm to be suitable for rib-rib, rib-spine and spine-spine constructions. Surgeons should be able to cut the rod to any desired length to adapt it for different patients.
- Be able to connect to the ribs and/or spine.
- Be single use. Therefore, sterilization will only be performed by the manufacturer.
- Be manufactured from biocompatible materials.
- Potentially be contoured to treat extreme kyphotic curvatures.
- Be designed as a single rod. However, its intended use can be as a pair of rods, depending on the patient's needs and surgeon's assessment.

3. INITIAL DESIGN

3.1. Description of the device

The novel device is an extendable implant composed of nine components (figure 2a): eight titanium alloy grade 5 (Ti-6Al-4V) parts and a component that can be either a compression spring or an elastomer. The implantation procedure is the same as for other growing rods; for further information see Miller and Vitale, (2016). However, the lengthening surgery can be performed in a minimally invasive way due to the elongation mechanism (figure 2b), which consists of a racked-rod and pinion self-locking system. The only manoeuvre required for surgeons to extend the device is a small incision through the skin and the insertion of a surgical tool which when turned clockwise elongates the device and self-locks. The surgical tool has a hexagonal profile with a distance across flats (A/F) of 4.2 mm (figure 2b). Hence, the required surgical incision for the elongation surgery is smaller than 5 mm. To offer the possibility to correct or reduce the length of elongation, another surgical tool can be inserted into the locking component to retract the rod. The device is curved with a radius of 220 mm (which is the same as the rod curvature of the VEPTR I device (DePuy Synthes Spine, 2015)) to better match the natural thoracic curvature of the spine in the sagittal plane and to minimize the need to contour the rod intraoperatively. Rod contouring has been reported to reduce the yield strength (Demura et al., 2015), fatigue strength (Lindsey et al., 2006) and endurance limits (Slivka and al., 2013) of titanium rods.

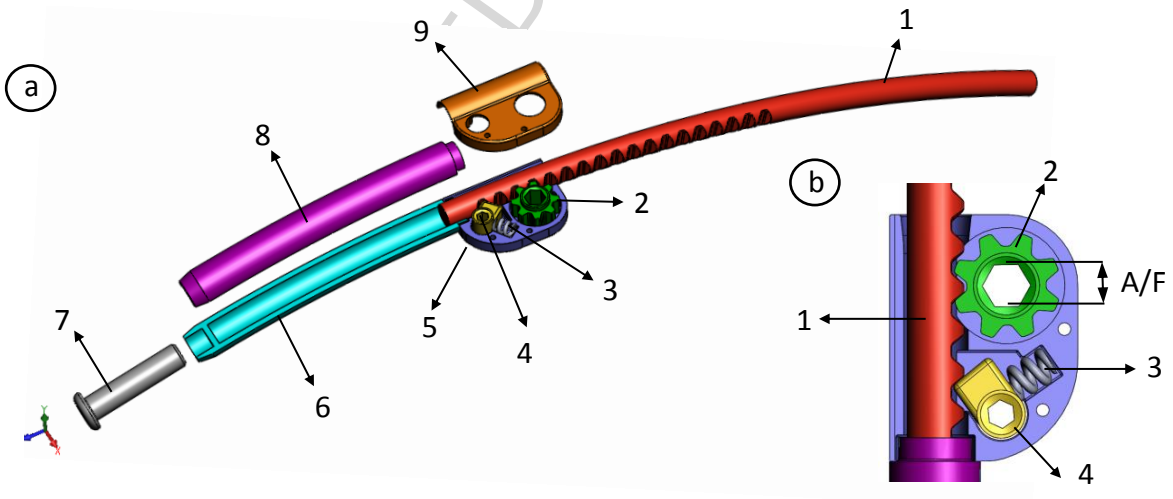

Figure 2*- Three-dimensional design of the device. a) Exploded view: 1: Racked-rod, 2: Pinion, 3: Compression spring, 4: Lock, 5: Lower case, 6: Lower body, 7: Bottom rod, 8: Upper body, 9: Upper case. b) Elongation mechanism without the upper case for visualization of the internal parts. The profile of the tool that is inserted into the pinion to elongate the rod has a distance across flats (A/F) of 4.2 mm.*

3.2. Evaluation

The most adverse scenario presented during the function of the device has been reported to occur when the rod is subjected to cyclic spinal compressive loads produced during flexion motion of the patient. Other in vivo loads did not produce comparable damage in the rods (Hill et al., 2017). These loads are transmitted from the upper anchor system (either a hook or screw) to the rod and then transferred to the lock, which prevents the sliding of the rod, and therefore becomes the most stressed component. In order to assess whether the design met strength requirements, finite element analysis (FEA) was performed under simulated flexion spinal loading.

3.2.1 Finite Element Analysis

The stress distribution of the device subjected to bending loads and extended at its maximum (presenting its worst case scenario) was simulated using Simlab 14.2 Software (Altair Engineering, Troy, Michigan, USA) after the parts were designed using SolidWorks 2014 (Dassault Systemes SolidWorks Corporation, Waltham, MA, USA). The spring and pinion components were neglected in the analysis as they performed their function during rod elongation and not in compression. The upper and lower bodies were combined in one part to simplify the simulation without compromising the results. All the components were modelled as Ti-6Al-4V, an isotropic, homogeneous and linearly elastic material with a Young's modulus of 110 GPa and a Poisson's ratio of 0.3 (Simoneau et al., 2017). A volume mesh was created by using second order tetrahedral elements. Mesh controls and refinements were assigned to topology entities where high stresses in the analysis were expected in order to have an accurate density, quality and structure of the mesh. All the parts had an element size ranging from 0.2 to 1.2 mm. Four mesh refinements were applied: (1) in the tooth of the rod being in contact with the lock; (2) in the locking part; and in the upper (3) and lower (4) cases where the lock was compressed against under compressive loads. The refinement element size was chosen based on a mesh convergence study in which differences in stresses were negligible with higher-density meshes. The total number of elements and element size for each component can be seen in table 1.

Table 1- *Number of elements and element size for the components of the meshed device.*

	COMPONENTS					
	RACK	***LOCK***	***UPPER CASE***	***LOWER CASE***	***COMBINED BODY***	***BOTTOM ROD***
N^o of Elements	31426	59810	6436	6502	5198	3746
Elem. Size (mm) General/refinement	0.9 / 0.2	0.2	1.2 / 0.3	1.2 / 0.3	1.3	0.9

Figure 3 shows the mesh and boundary conditions for the device simulations. A single force was applied on top of the rod where the pedicle screw or the rib hook would be assembled to the spine or rib. The force (figure 3a) was directed along the z-axis for several reasons: (1) to simulate bending compressive loads occurring during flexion motion of the patient, which represents the worst-case scenario for breakages of growing rods (Hill et al., 2017); (2) to mimic the loading scenario suggested by the ASTM F1717 Standard to test the rods; and (3) to direct the load to the elongation mechanism, where the highest stresses were expected. Various loading conditions were analysed: 100 N, 200 N, 300 N, 400 N and 500 N. The boundary conditions were defined, as shown in figure 3a, and including full constraints at the lowest surface of the implant. This was to simulate the attachment of the screw to the spine (figure 3a). All contacts were general except for a contact pair applied between the lock and rod components. 'Freeze' contacts (enforcing zero relative displacements on the contact interfaces) were used to represent welded joints between: the bottom rod with the body, the body with the upper case, the body with the lower case and the upper case with the lower case as shown in figure 3a and b. A 'stick' contact (the sliding phase is prevented) was defined for the rod tooth and lock coupling (figure 3b).

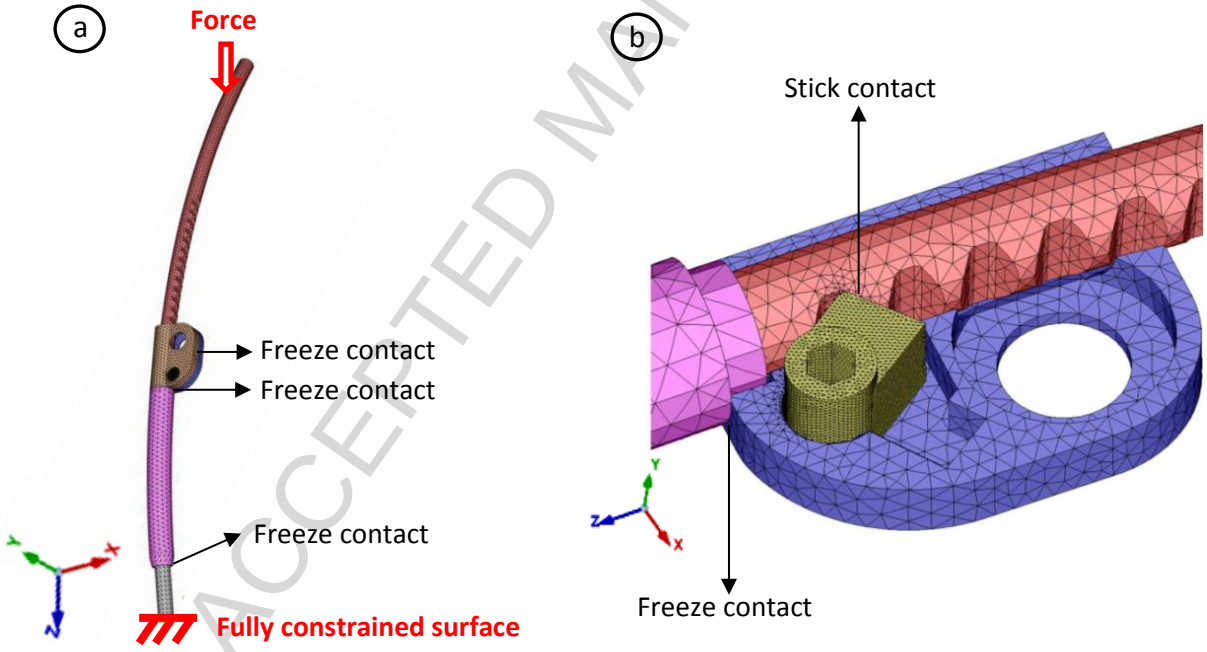

Figure 3- *Meshed device with applied compressive force and boundary conditions. a) Entire device with the indication of freeze contacts in between welded components, load and boundary conditions. b) Detailed view of the elongation mechanism without the upper case for visualization of the internal parts as well as the indication of the correspondent contacts between components.*

3.2.2. Results

The highest von Mises Stress (VMS) was found in the contact area between the rod and lock with the maximum value being in the rod for all loading conditions. The rest of the parts in the implant

showed considerably lower stresses in comparison with these components. The third most stressed part was the bottom rod followed by the lower and upper cases at the interfaces with the lock.

With forces of 100 N and 200 N, the maximum VMS was 303 MPa and 517 MPa, respectively, lower than the yield (847 MPa) and fatigue strength (620 MPa) of Ti-6Al-4V (Niinomi, 1998). Consequently, the device was considered to be safe both for static and fatigue compressive loads of up to 200 N. When loads increased to 300 N and 400 N, the maximum stress obtained reached 689 MPa and 812 MPa, respectively, lower values than the yield strength of the material, but higher than the fatigue endurance limit. Hence, the fatigue strength of the device was established to be between 200 and 300 N. When the implant was subjected to 500 N of load, the maximum VMS obtained was 929 MPa, exceeding the yield strength of the material. Hence, the yield strength of the device was established in between 400 and 500 N. It must be noted that the FE model guarantees a factor of safety as the load is fully taken by the implant, whereas in a clinical scenario the load is shared with the spine, ligaments, intervertebral discs, etc. (La Barbera et al., 2015).

Results of the stress distribution of the device subjected to a load of 200 N and 300 N can be seen in figures 4 and 5, respectively. A summary of the FEA results for all loading conditions is presented in table 2.

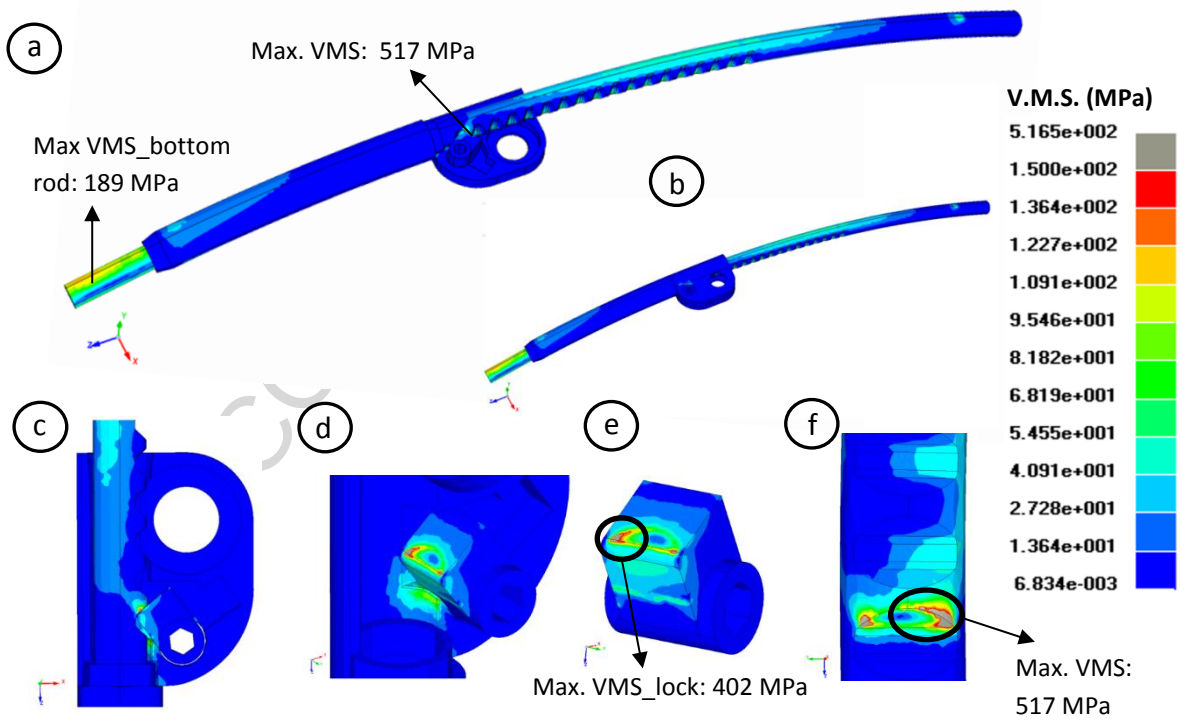

Figure 4*- Results of the von Mises Stress (VMS) distribution in MPa under 200 N of load. a) Entire device without upper case. b) Entire device with upper case. c) Elongation mechanism. d) Lock and lower case detail view. e) Lock component. f) Rod tooth, the most stressed part with 517 MPa.*

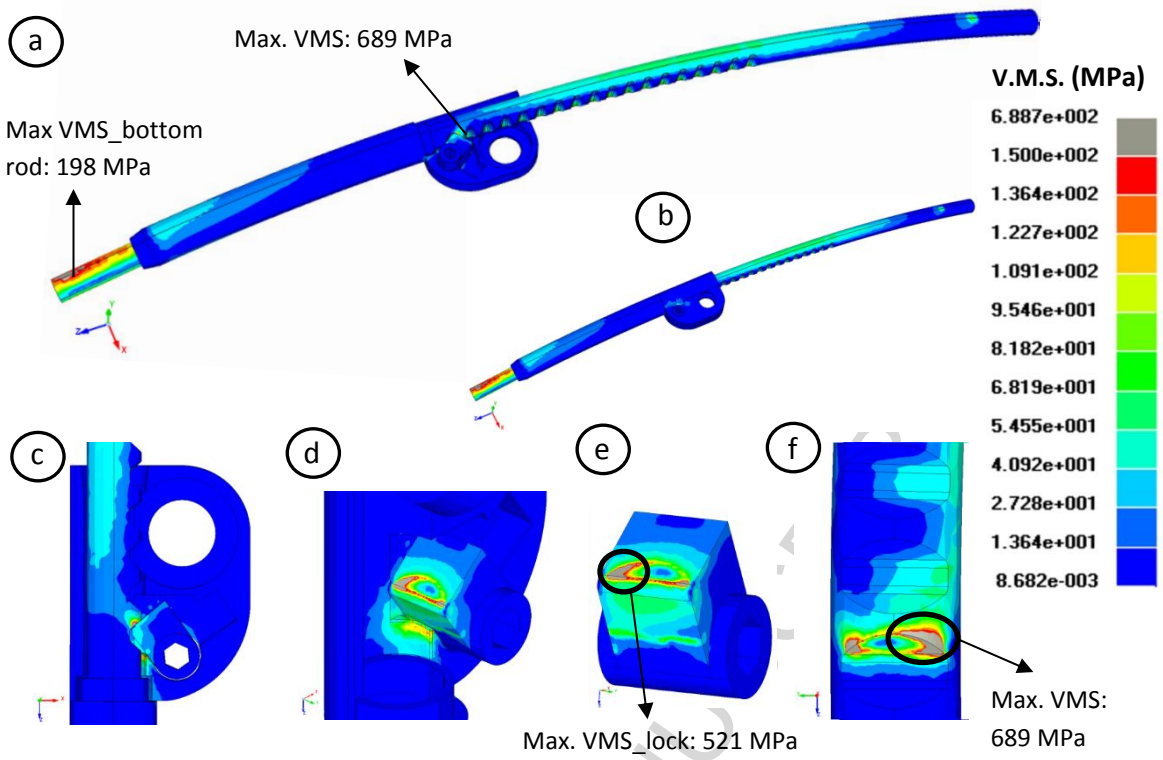

Figure 5- *Results of the von Mises Stress (VMS) distribution in MPa under 300 N of load. a) Entire device without upper case. b) Entire device with upper case. c) Elongation mechanism. d) Lock and lower case detail view. e) Lock component. f) Rod tooth, the most stressed part with 689 MPa.*

Table 2- *Summary of the stress distribution results of the device for all loading condition. VMS: von Mises Stress.*

Loads applied (N)	***Maximum VMS (MPa)***	***Maximum VMS vs Yield and Fatigue strength of Ti-6Al-4V***	***Comments***
100 N	303	*303 < 620 & 847*	Safe device under 100 N of static or fatigue compressive loads.
200 N	517	*517 < 620 & 847*	Safe device under 200 N of static or fatigue compressive loads, presenting an improved fatigue performance in comparison to VEPTR I (100 N of fatigue strength (FDA, 2004)).
300 N	689	*620 < 689 < 847*	Safe device under 300 N of static loads but unsafe under fatigue loading.
400 N	813	*620 < 813 < 847*	Safe device under 400 N of static compressive loads but unsafe under fatigue loading. This represents similar yield strength in comparison with VEPTR I (average ultimate load of 419 N (FDA, 2004)).
500 N	930	*620 & 847 < 930*	The device is not safe under 500 N of either static or fatigue compressive loads.

The results of the stress distribution analysis confirmed an improved mechanical performance of the device in comparison with the VEPTR I device. However, higher yield and fatigue strength was pursued for the novel device given the high rate of mechanical complications reported for VEPTR (Waldhausen et al., 2016) as well as the simplified loading condition that was analysed in the FEA.

4. FINAL DESIGN

In order to improve the mechanical compliance of the implant while keeping a low profile to meet dimensional requirements, a dynamic system was added to the bottom of the implant (which was the third most stressed component in the stress distribution analysis) close to the screw attachment, to avoid potential implant breakage (figure 6a). The dynamic system added was the BDyn device, a CE marked device commercially available from S14 Implants (Pessac, France) as a posterior dynamic stabilisation implant. The BDyn device consists of two elastomeric components (a polycarbonate urethane (PCU) ring and a silicone cushion), a mobile Ti-6Al-4V rod and a fixed rod made of the same material (figure 6b). The interaction of the mobile rod and the elastomeric components allows partial three-dimensional movement (Lawless et al., 2016). The device can rotate around its axis providing a polyaxiality of 14^{o} and can withstand axial loads up to 1 mm of displacement for traction and 2 mm for compression.

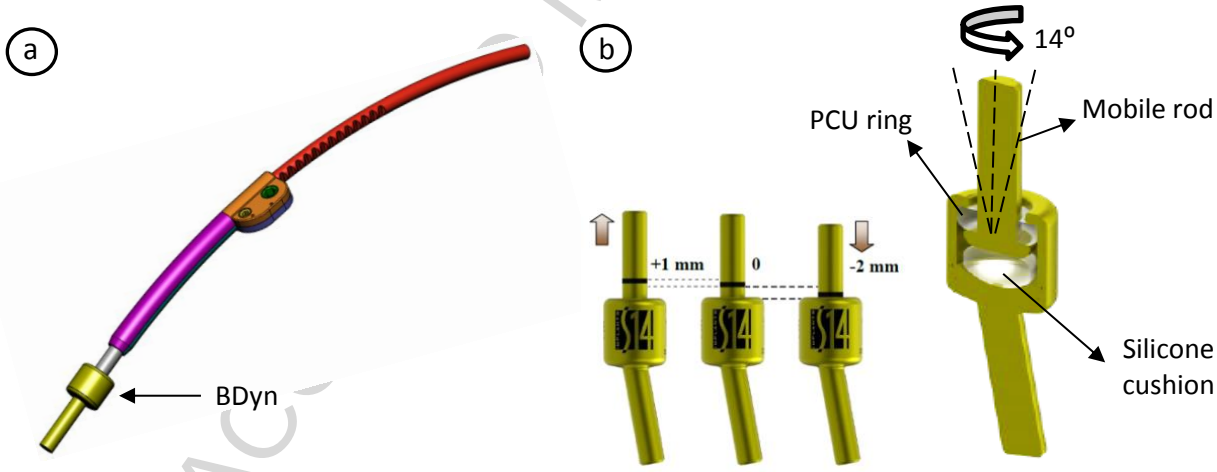

Figure 6*- a) Final design of the device with the addition of the dynamic system (BDyn). b) Motion range (tension, compression and polyaxiality) and cross section view of BDyn with its internal component: a polycarbonate urethane (PCU) ring and a silicone cushion.*

5. PROTOTYPE MANUFACTURE

Thirty one components (five of each of the following parts: lower case, upper case, lock, lower body, upper body and racked-rod as well as one pinion component) were milled on a 3-axis Computer Numerical Control (CNC) machine, deburred and given a light bead blast finish by Proto Labs Ltd.

(Telford, United Kingdom). The parts were made from Ti-6Al-4V to complete five working prototypes that would be mechanically tested under compression loads. The pinion delivered its function only during the distraction procedures and it was not needed in compression. Hence, only one pinion was manufactured to have one complete prototype that could be manually tested to verify its functioning during elongation of the rod.

The nine components composing one prototype (figure 7) include the milled Ti-6Al-4V parts as well as a stainless steel compression spring with a stiffness of 7.2 N/mm (Associated Spring Raymond, Worcestershire, UK) and a BDyn device. The five assemblies were prepared and laser welded (figure 8) by ABR Specialist Welding Ltd. (Birmingham, UK). Welding was applied in four areas following this chronological order: around the contact edges between upper and lower bodies; around the contact edges between bodies and cases; between upper and lower cases as well as BDyn and the bodies.

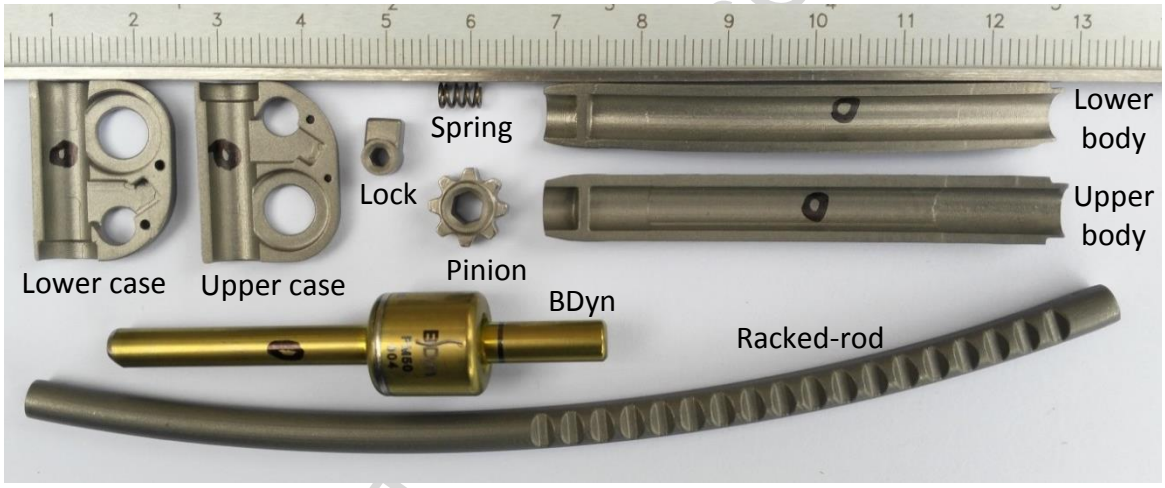

Figure 7- *The nine components composing one device: lower case, upper case, lock, compression spring, pinion, lower body, upper body, BDyn and racked-rod.*

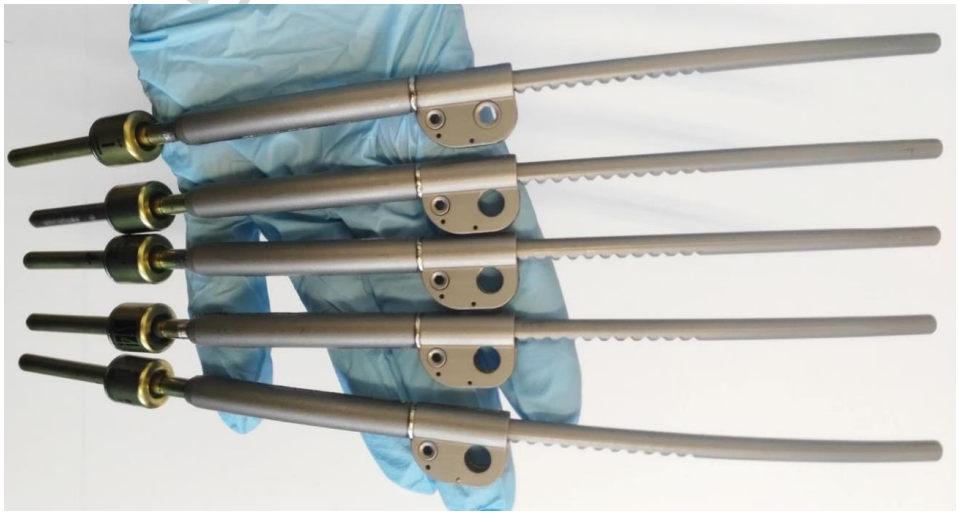

Figure 8- *The five prototypes of the implant after laser welding.*

6. PRECLINICAL EVALUATION

6.1. Test set up

In order to evaluate the stiffness and strength of the prototypes, compression bending quasi-static and fatigue tests were carried out. All mechanical testing was performed in ambient air using a Bose ElectroForce 3300 Series II Test Instrument running Win Test 4.1 software (Bose Corporation, Electroforce Systems Group, Minnesota, USA). Tests were conducted according to a modified version of ASTM F1717 (American Society for Testing and Materials, 2015) adapted to a paediatric thoracolumbar application with an active length between anchor points of 190 mm. In this configuration, the implant was extended to its maximum length and represented the worst-case scenario. Several jigs were designed and manufactured to assist in the testing of the prototypes. Ultra-High-Molecular-Weight-Polyethylene (UHMWPE) blocks were used to simulate a clinical scenario. The UHMWPE material was purchased from Direct plastics UK Ltd. (Cradley Heath, United Kingdom). The fixtures for the BOSE machine were designed to be U-shaped yokes from stainless steel. Two fixtures and seven pairs of UHMWPE blocks (which required replacement after each test) were produced. BFUS 2 pedicle screws (S14 Implants, Pessac, France) were used to anchor the prototypes to the UHMWPE blocks as the screws presented the stiffest construction in comparison with the hooks and, hence, the worst-case scenario for implant breakage to occur. The BFUS 2 were polyaxial screws with an outer diameter of 4.5 mm, an inner diameter of 3.1 mm, a shaft length of 45 mm and a thread length of 40 mm.

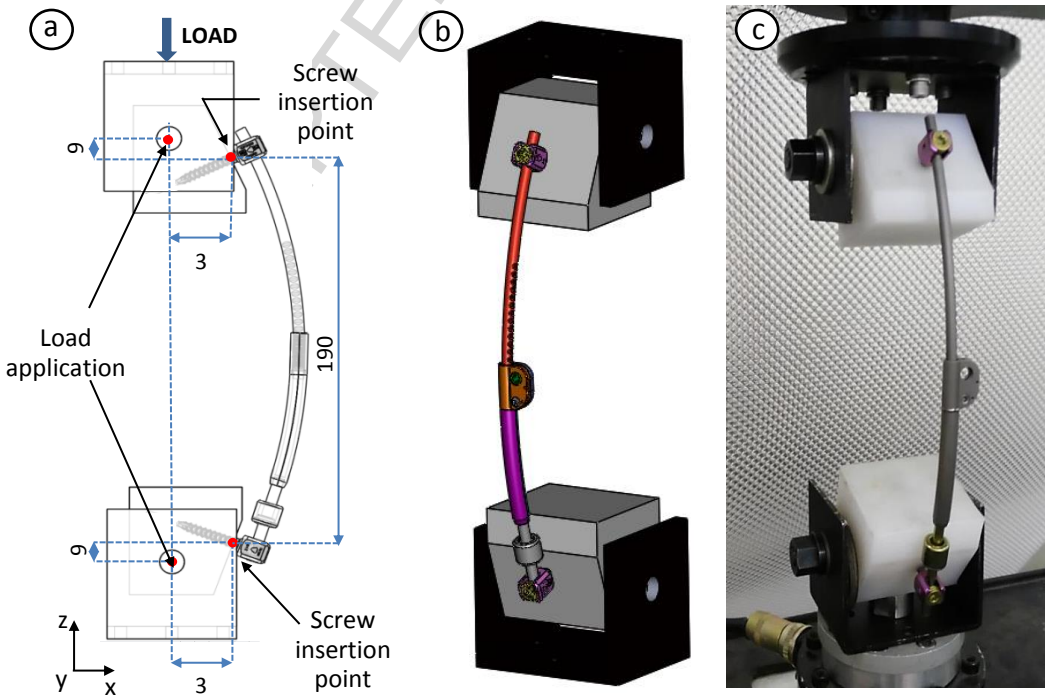

Figure 9- *Unilateral modified version of ASTM F1717 implant testing construction. a) Dimensions in mm. b) 3D CAD model. c) Manufactured parts and test assembly.*

6.2. Methods

6.2.1 Compression bending quasi-static tests

Ten quasi-static compression tests were conducted with one of the prototypes in order to obtain the yield strength of the spinal assembly and identify failure modes. Seven tests were carried out with the maximum active length. Three further tests were conducted with an active length of 130 mm (i.e. the device fully retracted) which modified the load path axially more directly into the elongation mechanism.

The first four quasi-static tests were carried out with rotating UHMWPE blocks, as suggested by the ASTM F1717. The rest of tests were performed with fixed UHMWPE blocks to allow the compression displacement to be fully taken by the prototype rather than partially by the rotation of the blocks. This was achieved by adding a welded plate to the back side of the U-shaped yokes with four screws and nuts, allowing to position the UHMWPE blocks at any desired angle and then to fix them with the screws.

Tests were performed at a displacement rate of 25 mm/min and load-displacement curves were obtained. The overall stiffness for each test was measured as the average slope of the curve.

6.2.2 Compression bending fatigue tests

Six fatigue bending compression tests were carried out in load control with five different prototypes. Tests were run with a preload of 50 N (determined from the quasi-static test results) to compensate for the clearances among the prototype components and simulate initial implantation. A sinusoidal load was applied that varied for each test. The fatigue strength was measured as the maximum load that was cyclically applied to the implant assembly at failure; runout was taken as 5 million cycles and the testing frequency was 5 Hz. The six tests were performed with an active length of 190 mm.

Fatigue tests 1, 2, 3, 5 and 6 were executed with the device extended so that the first tooth of the racked-rod was meshed with the lock (see figure 10a). The sinusoidal compressive load for these tests had the minimum and maximum values of: 10 and 100 N (fatigue 1); 100 and 180 N (fatigue 2 and 3); 120 and 200 N (fatigue 5); 110 and 190 N (fatigue 6). The loads for fatigue test 1 had a load ratio of 10 as suggested by ASTM F1717 Standard. The load ratio for the rest of test was less than 10 due to the limited stiffness of the compression spring of the elongation mechanism. A higher ratio would compress the spring and elongate the racked-rod. Therefore, for fatigue tests 2, 3, 5 and 6, the difference between minimum and maximum compressive sinusoidal loading was 80 N. For fatigue test 4, the device was tested with an extreme position of extension in which the first tooth of the rod meshed with the pinion, but not with the lock (see figure 10b). This configuration was tested as the spring was not used and, therefore, the load ratio of the cyclic loading could be increased. The

cyclic compressive loads applied for fatigue test 4 varied between 80 and 200 N. The total number of cycles to failure and the failure mode of each test were the two main results obtained for analysis.

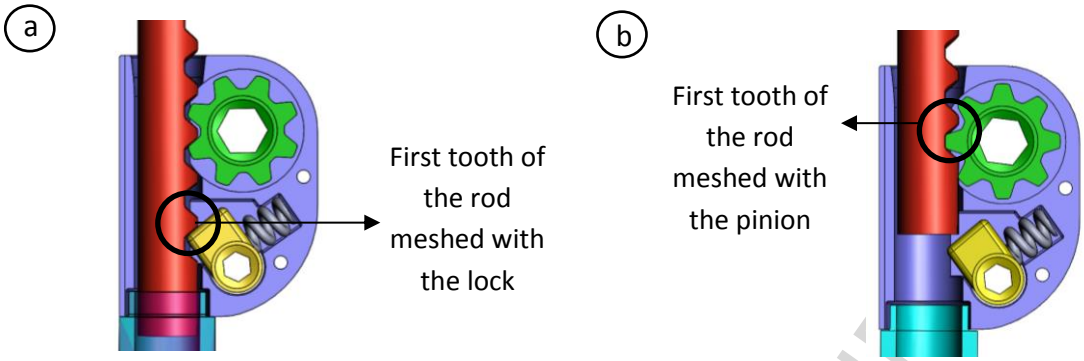

Figure 10- *Different configurations of the elongation mechanism during the fatigue tests. a) First tooth of the rod meshed with the lock for the fatigue tests 1, 2, 3, 5 and 6. b) Extreme position in which the first tooth of the rod meshed with the pinion but not with the lock during fatigue test 4.*

6.3. Results

6.3.1 Compression bending quasi-static tests

The results for the first 4 quasi-static tests are presented in figure 11. The four tests stopped when the machine reached its displacement limit. There were no failures or evidence of plastic deformation in any of the devices. A progressive increase in the preload after each test was applied due to the linear behaviour of the force and displacement curves which demonstrated that the device was working in its elastic range and the ultimate load was not obtained. In test 4, the progressive compression load caused some interference between the cylinder and the mobile rod of BDyn, changing the slope of the curve. This is marked with a black circle in figure 11.

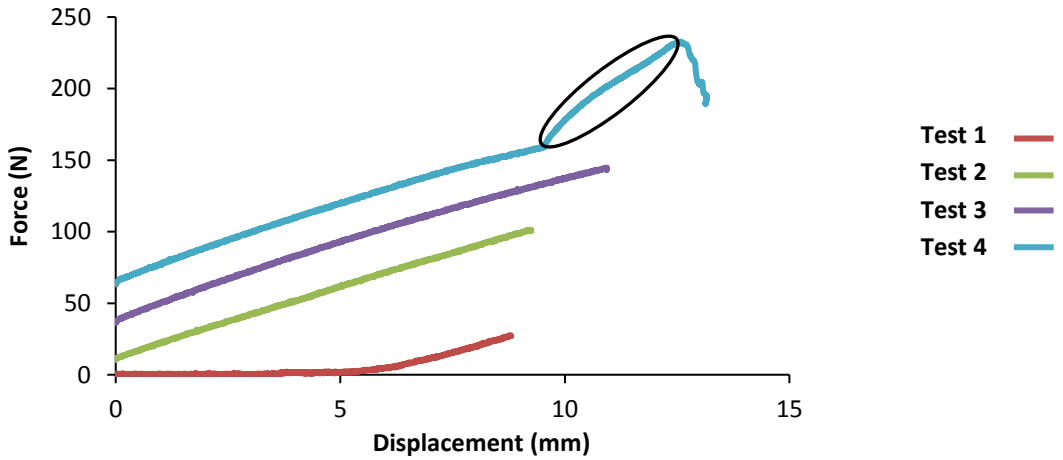

Figure 11- *Force and displacement curves of the four quasi-static compression bending tests 1, 2, 3 and 4 with an active length of 190 mm. The slope of each curve represents the stiffness in each test. The change in the slope caused by the interference between the BDyn components that occurred in test 4 is marked with a black circle.*

Another three quasi-static tests (test 5, 6 and 7) were performed with the fixed UHMWPE blocks and the results can be seen in figure 12. The three tests stopped when the maximum displacement was achieved and there was not any sign of failure in the prototype. The BDyn cylinder and mobile rod came into contact in test 7 due to the compressive load causing a change in the slope of the curve that is marked with a black circle in figure 12.

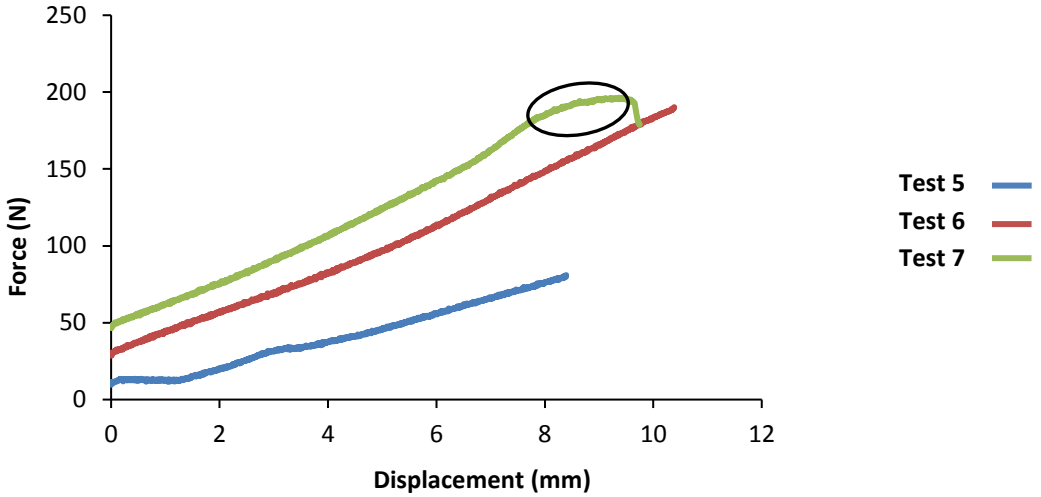

Figure 12- *Force and displacement curves of the three quasi-static compression bending tests 5, 6 and 7 with an active length of 190 mm. The slope of each curve represents the stiffness in each test. The change in the slope caused by the interference between the BDyn components that occurred in test 7 is marked with a black circle.*

The loads reached with the rod retracted were much higher (figure 13). The device did not show any sign of damage. The tests were judged to have failed as a result of slippage of the anchor system. The upper screw slipped in test 8 at 193.8 N and 6.5 mm of displacement, stopping the test. The lower screw slipped for test 9 at 296.5 N and 8.35 mm and for test 10 at 233.3 N and 7.71 mm. Test 9 and 10 reached maximum displacement after screw slippage. The trend of the three curves was linear except for when screw slippage occurred (which is marked with black circles in figure 13).

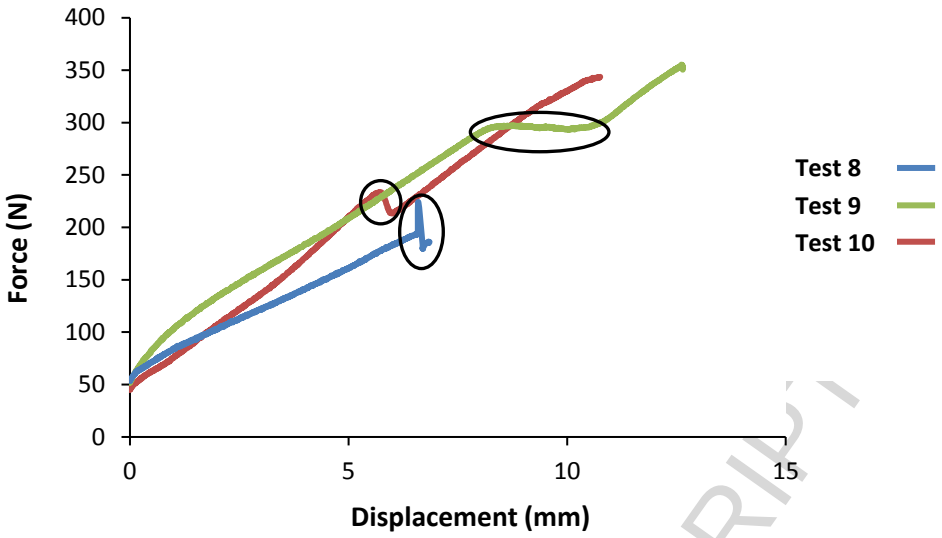

Figure 13- *Force and displacement curves of three quasi-static compression bending tests 8, 9 and 10 with an active length of 130 mm. The slope of each curve represents the stiffness in each test. The changes in the slope caused by the screw slippages in the three tests are marked with black circles.*

The yield strength was not obtained in any of the quasi-static tests as the prototype did not fail in any case (the failures for the retracted construction were anchor failures). The maximum load reached for the longest construction was 231.4 N and 357.3 N for the retracted position. The average stiffness of the first 4 quasi static tests was 9.4 N/mm. When repeating the same tests with the fixed UHMWPE blocks the stiffness increased by an average of 13.6 N/mm. The stiffness of the retracted position was higher with an average of 26.4 N/mm, very similar to the stiffness reported for VEPTR I device which was 26 N/mm (Food and Drug Administration, 2004). Table 3 summarises the results of the ten quasi-static compression tests along with the data from the VEPTR I device.

Table 3- *Summary of the results of the ten quasi-static compressing bending tests and data results from the VEPTR I device (Food and Drug Administration, 2004). T= Test.*

	T1	T2	T3	T4	T5	T6	T7	T8	T9	T10	VEPTR
Max. Load (N)	27.5	101.1	144.8	231.4	80.9	190.2	196.3	193.8	357.3	343.6	419
Stiffness (N/mm)	8.1	9.7	9.7	9.9	8.7	17.4	16.7	19.6	27.1	32.6	26

6.3.2 Compression bending fatigue tests

The first fatigue test ran out at 5 million cycles with the sinusoidal compressive loads of between 10 and 100 N. The second fatigue test was subjected to higher compressive loads of 100 and 180 N. This test stopped at 4 million cycles due to upper screw slippage. As there was not any sign of damage in the parts, the test was repeated with the same prototype and loading conditions. This test (fatigue test 3) ran out at 5 million cycles and, therefore, prototype 2 was subjected to 9 million cycles in total. The three following fatigue tests 4, 5 and 6, in which the peak load was raised to 200, 200 and 190 N, respectively, stopped due to lower screw failure that consisted of breakages at the neck of the screw and the interface of the UHMWPE blocks. One of the prototypes failed at a welding line with additional screw breakage. Consequently, the fatigue strength of the device for those failing tests was not obtained as the screw failures precluded implant failure. The fatigue strength of the device, or maximum load applied for 5 million cycles without failure, was 180 N in this study. Table 4 presents a summary of the testing results for the six fatigue tests performed.

Table 4*- Summary of the results for the fatigue tests 1, 2, 3, 4, 5 and 6.*

	LOAD (N)	LOADING RATIO	PROTOTYPE	CYCLES	FAILURE MODE
Fatigue 1	10, 100	10	1	5,000,000	No failure
Fatigue 2	100, 180	1.80	2	4,000,052	Upper screw slippage.
Fatigue 3	100, 180	1.80	2 (repeated)	5,000,000	No failure
Fatigue 4	80, 200	2.50	3	56,410	Lower screw breakage as well as welding breakage of device
Fatigue 5	120, 200	1.67	4	234,288	Lower screw breakage
Fatigue 6	110, 190	1.73	5	950,341	Lower screw breakage

Four tests stopped due to screw complications, consisting of one slippage (fatigue test 2) and three breakages (fatigue tests 4, 5 and 6) (figure 14a). One device broke at a weld line along with screw failure during fatigue test 4 (figure 14b). The fracture of the three pedicle screws occurred in the threaded shank close to the neck. Two ruptures were located in the second thread for fatigue test 4 and 5 and for fatigue test 6 the fracture happened in the third thread.

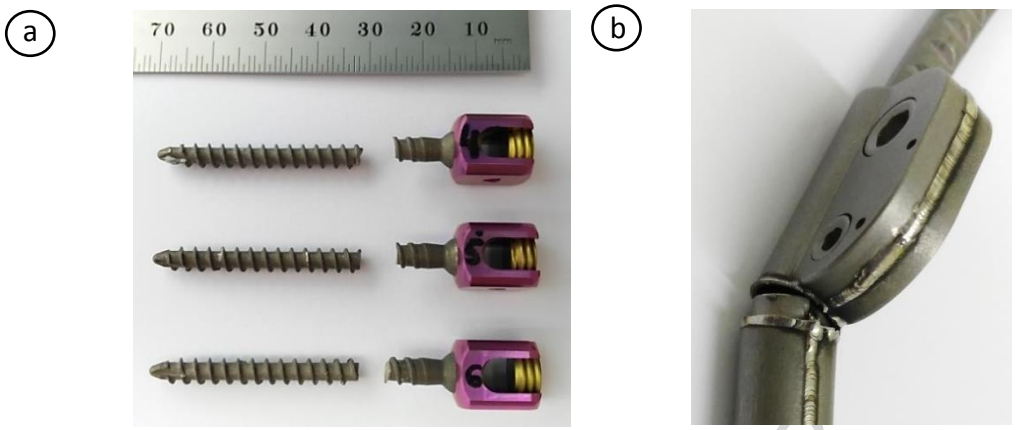

Figure 14- *Screw and welding fractures produced after fatigue testing. a) Fracture of three pedicle screws during fatigue tests 4, 5 and 6. b) Fracture of the device welding line after fatigue test 4.*

6.3.3 Fracture analysis

The fracture at the weld line occurred when the elongation mechanism was fixed in an extreme position of rod extension. This position should be avoided as the application of the load created a bending moment in the other extreme of the rod that pushed the upper case and caused the fracture of the weld line between the case and body. This pushing force was not produced during the rest of the fatigue tests as the elongation mechanism was more retracted and a part of the rod was enclosed within the bodies.

A failure analysis of the screw fracture surfaces was conducted using a low magnification stereomicroscope Wild M3Z (Wild Heerbrugg, Switzerland) with a Canon EOS 200D digital single-lens reflex camera and Cannon Capture software (Canon Inc., Tokyo, Japan) to confirm the failure mechanism. The breakages exhibited classical fatigue fractures and the three areas of a standard fatigue failure were identified: crack initiation (A), crack propagation (B) and brittle rupture (C). Optical microscope images of the screw fracture surfaces occurring in fatigue tests 4, 5 and 6 can be seen in figure 15 with a magnification of 10X.

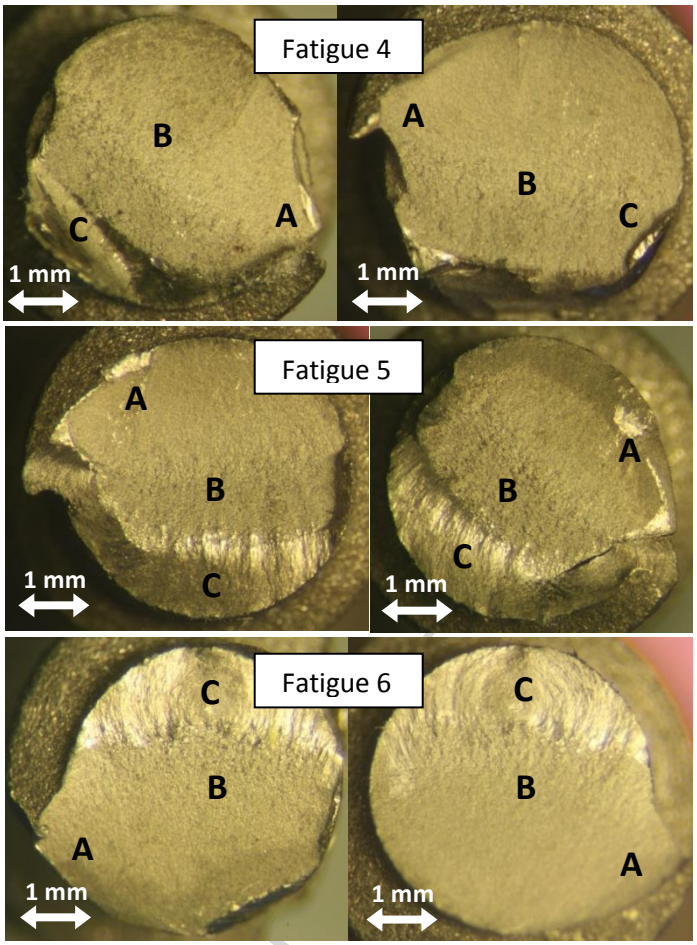

Figure 15- *Stereo microscope images (10X) of the pedicle screw fracture surfaces occurring in fatigue 4 (-80, -200 N and 56,410 cycles); fatigue 5 (-120, -200 N and 234,288 cycles); and fatigue 6 (-110, -190 N and 950,341 cycles). The standard fatigue fracture areas are marked as: (A) crack initiation, (B) crack propagation and (C) brittle fracture.*

7. DISCUSSION

This paper has presented the development of a novel growing rod that has been designed, evaluated, manufactured and mechanically tested. The device has been designed to address complications reported in current devices used for the surgical treatment of EOS. These features include a manually expandable device, avoiding reported difficulties with magnetically elongated implants such as the MAGEC device (Nuvasive Inc., San Diego, CA, USA). These complications comprise the failure of magnetic lengthening, fracture of the drive pin (Lebon et al., 2017; Teoh et al., 2016) and the provision of an uncontrolled elongation with the external remote. Lebon et al. (2017) reported in their multicentre study of 30 patients treated with MAGEC that the intended total length gain per patient was 40.1 mm, but the total measured length gain was 21.9 (45.5 % of reduction). The result of the design process is a device with two innovative features: (1) the lengthening mechanism that allows the elongation surgery to be performed manually in a minimally invasive way with a surgical incision of less than 5 mm (in comparison with the VEPTR device's

incision length of minimum 30 mm (Akbarnia et al., 2016)). This entails an easier and faster procedure when compared to other manually expanded implants and the potential to reduce skin and wound infections. Furthermore, the procedure could potentially be performed under local (rather than general) anaesthetic; and (2) the addition of a dynamic-viscoelastic system (BDyn implant) in the assembly aiming to improve the fatigue performance of the device and avoid rod breakages. The novel device designed is the first proposed scoliotic implant to include a dynamic component.

The implant was designed and analysed with FEA to anticipate the mechanical behaviour of the device under extreme operating conditions. The yield strength of the device resulted in a value between 400 and 500 N and a fatigue strength between 200 and 300 N. These are device properties that represent an improvement on data published on the state-of-the-art devices currently on the market such as the VEPTR I device. However, higher strength was pursued for the new device for two reasons: (1) the high rate of mechanical complications reported for VEPTR (Waldhausen et al., 2016); and (2) the FEA was performed with a simplified loading condition in which a single force was applied in the z direction whilst the real loading scenario in the body would be more complex with multidirectional loads being applied to the implant. Therefore, the stress distribution of the device was used as a design tool that led to the addition of a dynamic feature in the assembly (BDyn device).

Five working prototypes were manufactured and mechanically tested according to a modified version of the ASTM F1717 Standard. Quasi-static and fatigue compression-bending tests were performed to characterize the mechanical performance of the implant and assess its suitability for further clinical use. One prototype in this study reached five million cycles with the cyclic compressive loading reported as the fatigue strength for VEPTR I device: 10 N, 100 N (Food and Drug Administration, 2004). Another prototype withstood nine million cycles with higher compressive loads (peak load of 180 N) without any sign of damage to the implant. Therefore, the fatigue run-out loads for the novel implant in the tests conducted were greater than the reported run-out loads for the VEPTR I device. Three out of six fatigue tests did not achieve runout due to pedicle screw fracture with only one device failure along a welding line. The device did not reach higher fatigue strength of 180 N because the pedicle screws failed during the three fatigue tests where the loads were higher (190 and 200 N).

The quasi-static compression tests demonstrated that the device required a certain preload in order to compensate for the clearances within the device. In a clinical scenario, the device will always be pre-loaded by the weight of the patient and, hence, the application of the preload was justified. The

trend of the curves for all compression tests was linear except where screw failures or contact between BDyn components occurred. This is indicative of the device remaining within its elastic limits during the quasi-static tests.

Fractures in growing rods usually occur in one of three rod locations: mid-construct, adjacent to tandem connectors or close to the distal anchor point (Hill et al., 2017; Yang et al., 2011; Yamanaka et al., 2015). This was not the case in the fatigue tests of this study where failure occurred in the screws rather than in the device. One fracture occurred in a welding line whilst none of the rods showed any sign of failure. This may be due to the incorporation of the BDyn dynamic stabilisation system, which was added with the purpose of reducing dynamic loads through compliance in the implant construction. Yamaguchi et al. (2014) suggested that less rigid constructions are associated with less rod breakages. Sankar et al. (2010) reported that hybrid constructions (the most flexible ones in which the implant is attached to the patient with pedicle or rib hooks instead of screws) cause less implant complications. In this study, the flexible device concentrated the fluctuating bending stresses on the anchor points and not in the rod. There were no rod failures during testing which may prevent implant breakage and, consequently, emergency surgeries. Furthermore, the addition of BDyn is expected to reduce the stresses induced at the contact surface between lock and rod, decreasing the chance of wear debris being generated between these titanium alloy parts.

This is the first dynamic growing rod that has been designed and tested following a modified version of the ASTM F1717 Standard but other authors such as Slivka et al (2013) and Jager et al. (2015) have used this Standard to evaluate spinal rods. In this study, modifications were made to account for paediatric patients and the flexibility of the BDyn device. These included preventing the UHMWPE blocks from rotating as well as changing the assembly set up parameters to account for a single implant testing. All modifications were made with consideration to La Barbera et al. (2014) recommendations.

Four screw failures occurred, one slippage and three breakages. One breakage occurred at the third thread of the shank at the peak load of 190 N and two breakages at the second thread at the peak load of 200 N. This could be due to the fact that at this point of the shank the inner diameter of the screw changes. Furthermore, the root for the screw thread is characterized by a sharp edge instead of a fillet which could prevent stress concentrations. These results suggested the need to redesign the BFUS 2 pedicle screw model (S14 Implants, Pessac, France) if they are to be used for clinical implantation with the growing rod. If further mechanical tests are to be completed to evaluate the novel growing rod, larger diameters for the screw may be considered as well as using a different screw model from another manufacturer.

The number of prototypes tested was limited and the results cannot be considered to be statistically significant. However, the tests demonstrated the mechanical behaviour of the implant. More prototypes would be evaluated to confirm the results and before clinical trials. Furthermore, tests following the ASTM F1717 are performed with simplified loading configurations and the results obtained are unlikely to predict in-vivo performance. Nevertheless, this Standard guarantees a coefficient of safety (La Barbera et al., 2015) as the load is fully taken by the spinal construction and it is not shared with any anterior support (vertebrae, intervertebral discs, ligaments, etc.) as occurs in the body. Hill et al. (2017) reported that rod fractures with growing rods are caused by repeated flexion motion and other in vivo loads did not produce comparable damage in the rods. In the present study, both the FEA and the mechanical tests were performed with the device subjected to simulated flexion bending loads as well as extended to the maximum length. Therefore, the analyses presented the worst-case scenarios. The novel implant proved better long term behaviour than VEPTR I device, which has been implanted in patients since 2002 (Campbell, 2013). Therefore, despite further mechanical testing being required to confirm the benefits stated above, the device has clinical potential to progress towards implantation.

8. CONCLUSIONS

This paper describes the development of a dynamic implant designed to correct three dimensional spinal deformities in children with Early Onset Scoliosis (EOS). The key features of the paper are:

- The novel distraction-based implant included a compliant viscoelastic component that provides protection against dynamic device fractures, and a novel minimally invasive lengthening mechanism, reducing infection.
- The device was designed and evaluated first with finite element analysis, and then physically tested, using a modified version of the ASTM F1717 Standard.
- Results demonstrated an improved fatigue performance in comparison to a current market leading EOS implant.
- Novel device proposed has the clinical potential to improve the surgical treatment of EOS.

Acknowledgements

The authors would like to thank Frederic Fortin, Johann Robin and Brice Sennequier for their general guidance during the development of the project as well as Carl Hingley, Lee Gauntlett, Peter Thornton and Jack Garrod from the Department of Mechanical Engineering, University of Birmingham for manufacture of fixtures and design guidance. This research was supported by the European Commission under the 7th Framework Programme (Grant agreement no.: 604935).

Data Availability

The raw/processed data required to reproduce these findings cannot be shared at this time due to legal or ethical reasons.

REFERENCES

Akbarnia, B. A., Marks, D. S., Boachie-Adjei, O., Thompson, A. G., & Asher, M. A. (2005). Dual growing rod technique for the treatment of progressive early-onset scoliosis: a multicenter study. *Spine*, *30*(17S), S46-S57.

Akbarnia, B. A., Breakwell, L. M., Marks, D. S., McCarthy, R. E., Thompson, A. G., Canale, S. K., ... & Growing Spine Study Group. (2008). Dual growing rod technique followed for three to eleven years until final fusion: the effect of frequency of lengthening. *Spine*, *33*(9), 984-990.

Akbarnia, B. A., Yazici, M., & Thompson, G. H. (Eds.). (2016). *The growing spine: management of spinal disorders in young children*. Springer Science & Business Media.

ASTM International F1717-15 (2015). Standard Test Methods for Spinal Implant Constructs in a Vertebrectomy Model.

Campbell, R. M. (2013). VEPTR: past experience and the future of VEPTR principles. *European Spine Journal*, *22*(2), 106-117.

Cunin, V. (2015). Early-onset scoliosis–current treatment. *Orthopaedics & Traumatology: Surgery & Research*, *101*(1), S109-S118.

Demura, S., Murakami, H., Hayashi, H., Kato, S., Yoshioka, K., Yokogawa, N., ... & Tsuchiya, H. (2015). Influence of rod contouring on rod strength and stiffness in spine surgery. *Orthopedics*, *38*(6), e520-e525.

Depuy Synthes Spine. (2016) VEPTR Surgical Technique. Available from: http://synthes.vo.llnwd.net/o16/LLNWMB8/INT%20Mobile/Synthes%20International/Product%20Support%20Material/legacy_Synthes_PDF/DSEM-SPN-1215-0398_LR.pdf [Accessed 19th May 2018].

Depuy Synthes Spine. (2015). VEPTR II Titanium Rib, Surgical Technique. Available from: http://sites.synthes.com/mediabin/US%20DATA/Product%20Support%20Materials/Technique%20Guides/DSUSSPN11140557_VEPTR_II_TG.pdf [Accessed 17th October 2017].

Food and Drug Administration (2004). Summary of safety and probable benefit data of VEPTR. Available from: https://www.fda.gov/ohrms/dockets/dailys/04/sep04/091504/04m-0415-aav0001-03-SSED-vol1.pdf [Accessed 24th July 2017].

Greggi, T., Lolli, F., Di Silvestre, M., Martikos, K., Vommaro, F., Maredi, E., ... & Cioni, A. (2012). Complications incidence in the treatment of early onset scoliosis with growing spinal implants. *Studies in Health Technology and Informatics, 176*, 334-337.

Hill, G., Nagaraja, S., Akbarnia, B. A., Pawelek, J., Sponseller, P., Sturm, P., ... & Dreher, M. (2017). Retrieval and clinical analysis of distraction-based dual growing rod constructs for early onset scoliosis. *The Spine Journal*, *17*(10), 1506-1518

Jager, Z. S., İnceoğlu, S., Palmer, D., Akpolat, Y. T., & Cheng, W. K. (2016). Preventing instrumentation failure in three-column spinal osteotomy: biomechanical analysis of rod configuration. *Spine Deformity*, *4*(1), 3-9.

Karol, L. A., Johnston, C., Mladenov, K., Schochet, P., Walters, P., & Browne, R. H. (2008). Pulmonary function following early thoracic fusion in non-neuromuscular scoliosis. *The Journal of Bone & Joint Surgery, 90*(6), 1272-1281.

La Barbera, L., Galbusera, F., Villa, T., Costa, F., & Wilke, H. J. (2014). ASTM F1717 standard for the preclinical evaluation of posterior spinal fixators: Can we improve it?. *Proceedings of the Institution of Mechanical Engineers, Part H: Journal of Engineering in Medicine*, *228*(10), 1014-1026.

La Barbera, L., Ottardi, C., & Villa, T. (2015). Comparative analysis of international standards for the fatigue testing of posterior spinal fixation systems: the importance of preload in ISO 12189. *The Spine Journal*, *15*(10), 2290-2296.

Lawless, B. M., Barnes, S. C., Espino, D. M., & Shepherd, D. E. (2016). Viscoelastic properties of a spinal posterior dynamic stabilisation device. *Journal of the Mechanical Behavior of Biomedical Materials*, *59*, 519-526.

Lebon, J., Batailler, C., Wargny, M., Choufani, E., Violas, P., Fron, D., ... & De Gauzy, J. S. (2017). Magnetically controlled growing rod in early onset scoliosis: a 30-case multicenter study. *European Spine Journal*, *26*(6), 1567-1576.

Lindsey, C., Deviren, V., Xu, Z., Yeh, R. F., & Puttlitz, C. M. (2006). The effects of rod contouring on spinal construct fatigue strength. *Spine*, *31*(15), 1680-1687.

Miller, D. J., & Vitale, M. G. (2016). Rib-Based Anchors for Growing Rods in the Treatment of Early-Onset Scoliosis. *Operative Techniques in Orthopaedics*, 26(4), 241-246.

Niinomi, M. (1998). Mechanical properties of biomedical titanium alloys. *Materials Science and Engineering: A*, *243*(1), 231-236.

Odent, T., Ilharreborde, B., Miladi, L., Khouri, N., Violas, P., Ouellet, J., ... & Scoliosis Study Group. (2015). Fusionless surgery in early-onset scoliosis. *Orthopaedics & Traumatology: Surgery & Research*, *101*(6), S281-S288.

Oetgen, M. E., & Blakemore, L. C. (2012). Growing Rods in Early-Onset Scoliosis. In *Seminars in Spine Surgery. 24*(3), 155-163. WB Saunders.

Sankar, W. N., Acevedo, D. C., & Skaggs, D. L. (2010). Comparison of complications among growing spinal implants. *Spine*, *35*(23), 2091-2096.

Simoneau, C., Terriault, P., Jetté, B., Dumas, M., & Brailovski, V. (2017). Development of a porous metallic femoral stem: Design, manufacturing, simulation and mechanical testing. *Materials & Design*, *114*, 546-556.

Slivka, M. A., Fan, Y. K., & Eck, J. C. (2013). The effect of contouring on fatigue strength of spinal rods: is it okay to re-bend and which materials are best?. *Spine Deformity*, *1*(6), 395-400.

Teoh, K. H., Winson, D. M., James, S. H., Jones, A., Howes, J., Davies, P. R., & Ahuja, S. (2016). Do magnetic growing rods have lower complication rates compared with conventional growing rods?. *The Spine Journal*, *16*(4), S40-S44.

Thompson, G. H., Akbarnia, B. A., Kostial, P., Poe-Kochert, C., Armstrong, D. G., Roh, J., ... & Marks, D. S. (2005). Comparison of single and dual growing rod techniques followed through definitive surgery: a preliminary study. *Spine*, *30*(18), 2039-2044.

Waldhausen, J. H., Redding, G., White, K., & Song, K. (2016). Complications in using the vertical expandable prosthetic titanium rib (VEPTR) in children. *Journal of Pediatric Surgery*, *51*(11), 1747-1750.

Yamaguchi, K. T., Skaggs, D. L., Mansour, S., Myung, K. S., Yazici, M., Johnston, C., ... & Growing Spine Study Group. (2014). Are rib versus spine anchors protective against breakage of growing rods?. *Spine Deformity*, *2*(6), 489-492.

Yamanaka, K., Mori, M., Yamazaki, K., Kumagai, R., Doita, M., & Chiba, A. (2015). Analysis of the fracture mechanism of Ti-6Al-4V alloy rods that failed clinically after spinal instrumentation surgery. *Spine*, *40*(13), E767-E773.

Yang, J. S., Sponseller, P. D., Thompson, G. H., Akbarnia, B. A., Emans, J. B., Yazici, M., ... & Growing Spine Study Group. (2011). Growing rod fractures: risk factors and opportunities for prevention. *Spine*, *36*(20), 1639-1644.

Yang, S., Andras, L. M., Redding, G. J., & Skaggs, D. L. (2016). Early-onset scoliosis: a review of history, current treatment, and future directions. *Pediatrics*, *137*(1), e20150709.

Choudhury, M. Z. B., Tsirikos, A. I., & Marks, D. S. (2017). Early-onset scoliosis: clinical presentation, assessment and treatment options. *Orthopaedics and Trauma*, *31*(6), 357-363.

Graphical abstract

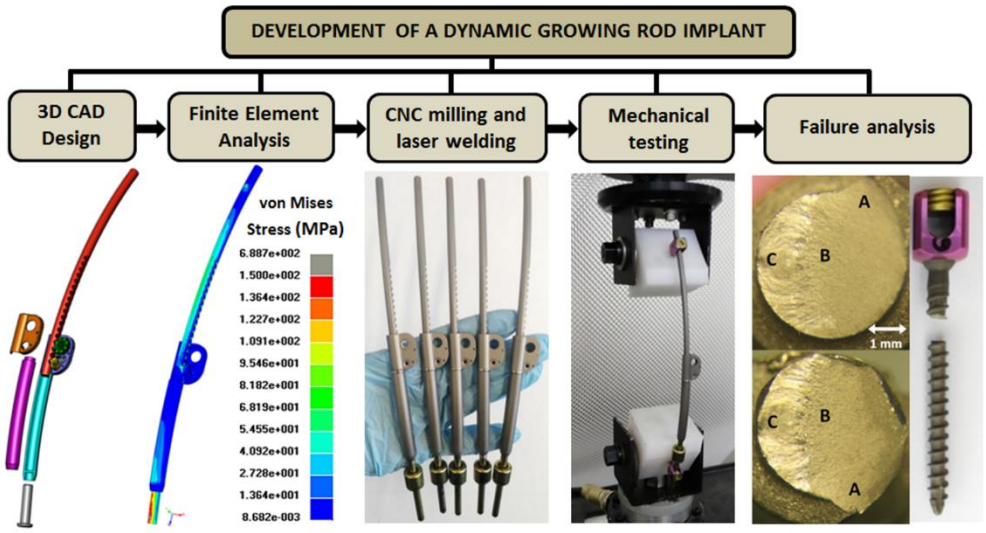

Highlights

- *A novel dynamic growing rod that aims to improve the surgical treatment of early onset scoliosis has been developed.*
- *The implant includes a dynamic system that was added after a stress distribution analysis was undertaken using finite element analysis.*
- *Five working prototypes were manufactured in titanium alloy that were mechanically tested in quasi-static and fatigue compression bending.*
- *Experimental tests results demonstrated that the implant provides an improved fatigue performance in comparison with a current marketed device.*